Available online at www.sciencedirect.com
ScienceDirect
Physica A 386 (2007) 666–673
PHYSICA A
www.elsevier.com/locate/physa

# Structural complexity of disordered surfaces: Analyzing the porous silicon SFM patterns

R.R. Rosa[a,*], M.P.M.A. Baroni[a], G.T. Zaniboni[b], A. Ferreira da Silva[c], L.S. Roman[d], J. Pontes[e], M.J.A. Bolzan[f]

[a] *Núcleo para Simulação e Análise de Sistemas Complexos, Laboratório Associado de Computação e Matemática Aplicada (LAC), Instituto Nacional de Pesquisas Espaciais (INPE), S.J. dos Campos, SP, Brazil*
[b] *Instituto de Física, Instituto Tecnológico de Aeronáutica (ITA), S.J. dos Campos, SP, Brazil*
[c] *Instituto de Física, Universidade Federal da Bahia, Salvador, BA, Brazil*
[d] *Departamento de Física, Universidade Federal do Paraná, Curitiba, PR, Brazil*
[e] *COPPE, Universidade Federal do Rio de Janeiro, Rio de Janeiro, RJ, Brazil*
[f] *IP&D, Universidade do Vale do Paraíba (UNIVAP), S.J. dos Campos, SP, Brazil*

Available online 6 September 2007

## Abstract

This paper introduces a relative structural complexity measure for the characterization of disordered surfaces. Numerical solutions of 2d + 1 KPZ equation and scanning force microscopy (SFM) patterns of porous silicon samples are analyzed using this methodology. The results and phenomenological interpretation indicate that the proposed measure is efficient for quantitatively characterize the structural complexity of disordered surfaces (and interfaces) observed and/or simulated in nano, micro and ordinary scales.
© 2007 Elsevier B.V. All rights reserved.

*Keywords:* Disordered surfaces; Structural complexity; Gradient pattern analysis; Wavelet multiresolution analysis; Euler characteristic; KPZ equation; Porous silicon

## 1. Introduction

Usually the formation of surfaces is influenced by a large number of factors, where randomness plays an essential role in shaping the final morphology of a given surface or interface. Thus, the characterization of morphological structures and the related dynamics of growth and/or deposition is remarkably challenging in the modern field of *physical morphometry* [1–4]. In the branch of nanometric disordered structures, the problem becomes worse due to limitations in obtaining and visualizing confident samples where the complex local patterns are represented by the real spatio-temporal scales and scaling relations. This is an important limitation in statistical physics and several roughening processes are described using scaling concepts. One essential property of scaling relations in complex surfaces is the universality class, from where scaling exponents are related through scaling laws, which represent an essential link between experimental samples

*Corresponding author. Tel.: +55 12 3945 6534; fax: +55 12 3945 6375.
*E-mail address:* reinaldo.rosa@pq.cnpq.br (R.R. Rosa).

0378-4371/$ - see front matter © 2007 Elsevier B.V. All rights reserved.
doi:10.1016/j.physa.2007.08.044

and theoretical models [5]. In particular, for the field of disorderly surface formation, there are a number of simulation studies (e.g., Refs. [6–8]) where the most successful theoretical approach is based on stochastic differential equations, especially the so-called KPZ equation [9] as the most usable one.

Recently, the KPZ equation has been used to model the surface of porous silicon [10], where a quantitative description of porous silicon morphology and its correlation with optical properties, measured from real samples, were investigated. The complex surface characterization was performed through the so-called gradient pattern analysis (GPA) methodology [2,3,11–17]. Analysis of scanning force microscopy (SFM) images of porous silicon fabricated by electrochemical etching was able to verify that photoluminescence (PL) performance is not exclusively dependent on the amount of roughness (or surface porosity), but it is also dependent on the porous surface morphology [16,17]. The analysis of the modeled surfaces showed that it is possible to reproduce, with good approximation, the disordered character of the porous surfaces by means of the $2d+1$ numerical solution of KPZ equation [10,18].

Taking into account the morphology influence on the porous silicon PL performance, we interpret the morphological analysis as a complementary approach to the conventional dynamical characterization based on scaling exponents. It is important to note that, up to the moment, there is no real experiment from where one can follow the growth dynamics of nanometric porous surface in substrates as Si crystals; therefore, for surface formation based on real silicon substrate samples, the growth exponent is still unknown. Due to this limitation, based on conventional scaling analysis for porous silicon surface, here we introduce a complementary methodology to improve the characterization of disordered porous nanometric surfaces. This is based on the concept of *relative structural complexity*, $\rho_{SC}$, introduced in Section 3 of this paper. This measure congregates mutual information distances from three distinct approaches: integral geometry (*Euler characteristic*), convex geometry (*gradient asymmetry*) and algebraic orthogonal transformation (*2D wavelet decomposition*).

## 2. Experimental and numerical data

### 2.1. Porous silicon samples

The porous silicon samples, SP83 and SP101 (see Fig. 1a and b), were produced by anodic etching of crystalline silicon wafers in hydrofluoric (HF) acid solution. The surface modification procedures have directed towards improving the material optical properties. More experimental details are given by Ferreira da Silva et al. (2000). These samples were analyzed by SFM to obtain the morphology of the porosity. The SFM measurements were performed using the Digital Instruments Nanoscope III running in tapping mode. In this imaging mode, the SFM tip-cantilever oscillated sinusoidally at high frequencies (w300 kHz) amplitude (10–100 nm), so that the tip contacted the surface once during each period. Scans were made over areas from $500 \times 500$ nm till $20 \times 20$ mm with a resolution of $512 \times 512$ pixels and with the scan rate of 1–2 Hz. Table 1 lists the main characteristics of these samples: the PL energy, the size of horizontal local structures ($h$), the size of vertical local structures ($\Gamma_0$), the roughness coefficient ($W$) and the average level of asymmetry ($\langle g_A \rangle$) due to the presence of walls and valleys [10,18].

The emphasis here is on the characterization of a relative structural complexity of porous silicon samples and possible correspondent generic models. For this purpose was considered, for comparison criteria in nanoscales, a reference sample (GM08) of Au film deposited under ultra-high vacuum conditions on air-cleaved mica substrate, called here Au-on-Mica (Fig. 1c). Mica is the most suitable substrate for gold epitaxial deposition since its crystallographic parameters are close to gold crystal parameters [19]. The exposition in situ to Hg vapor led to transformation of continuous gold film into isolated amalgam walls of nanometer scale ($\sim$100 nm) that were visualized by the atomic force microscopy method, showing scaling sizes compatible to our porous silicon samples.

### 2.2. Simulated surface

In this work, we also analyzed a model surface based on the $2d+1$ solutions of KPZ equation. Simulations of the KPZ equation, for 2D nano-lattices, have shown good agreement with the standard expected

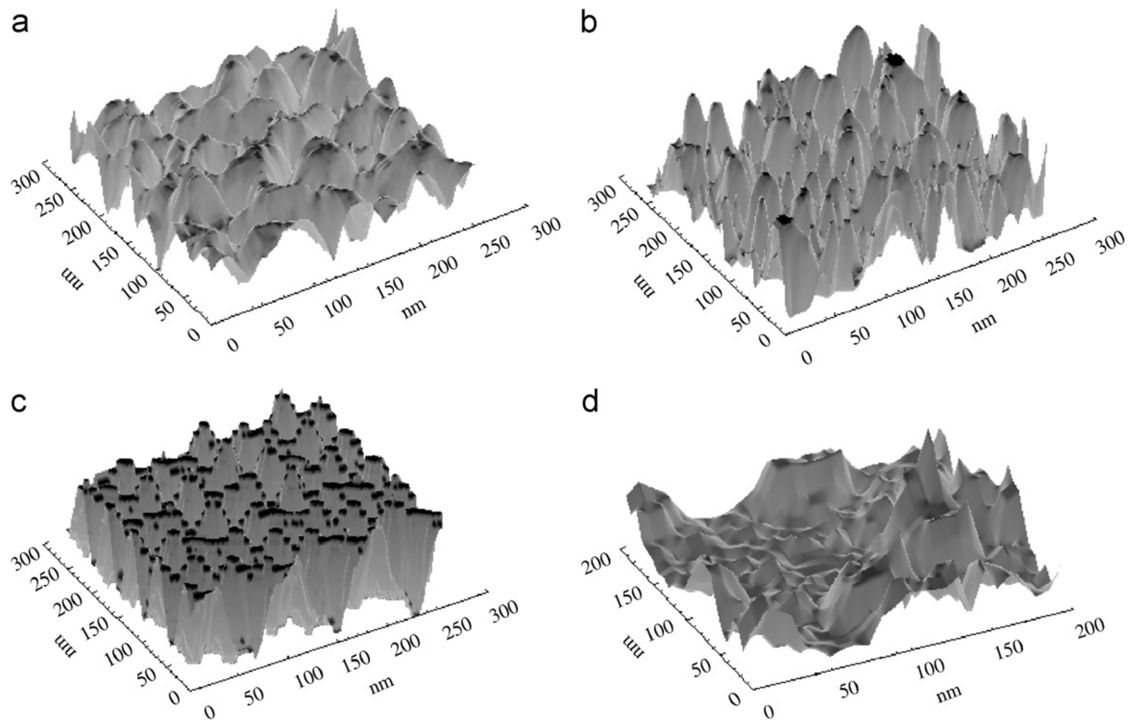


Fig. 1. (a) Psi SFM surface from sample SP-83 (low roughness); (b) Psi SFM surface from sample SP-101 (high roughness); (c) a regular gold-on-mica deposition surface showing low structural complexity, Au–Mica, from sample GM08; (d) a typical nKPZ surface ($193 \times 193$) with $\upsilon = -0.2$, $\sigma = 1$ and $\lambda = 3$. The images are all in normalized nanometer (nm) scale ranging from: 1 to 256 nm for a, b and c, and from 1 to 193 nm for *d*, in the *xy* plane. The amplitude are plotted in a 1–20 nm normalized vertical range.

Table 1
Measured characteristics of the porous silicon samples showed in Fig. 1a and b, SP083 and SP101, respectively. Here, $g_A$ is the first gradient moment $g_1$ written in terms of percentage of asymmetry (see [10,15])

| Sample | $E$ (eV) | $h$ (nm) | $\Gamma_0$ (nm) | $W$ (%) | $\langle g_A \rangle$ (%) |
|---|---|---|---|---|---|
| SP083 | 1.83 | 8–10 | 30–60 | 52 | 0.68 |
| SP101 | 1.73 | 8–12 | 5–50 | 74 | 0.62 |

scaling exponents ($\alpha = 0.34$ and $\beta = 0.24$). This approach is appropriate because we are interested not only in the morphology of the final surface, but also in the dynamics of how the morphology develops in time.

The KPZ equation, in 1d + 1 dimension, is given by the following expression:

$$\frac{\partial h(x,t)}{\partial t} = \upsilon \nabla^2 h + \frac{\lambda}{2}(\nabla h)^2 + \eta(x,t), \qquad (1)$$

where $h(x,t)$ is the height (position $x$, time $t$), $\upsilon$ is the surface tension, $\lambda$ is the parameter of lateral growth and $\eta(x,t)$ is the noise term. A result from 2d + 1 KPZ simulation, solved by means of the FTCS (forward time centered space) method, is shown in Fig. 1d, where the sub-samples lattice scales ($193 \times 193$) are compatible to scales of 1 nm per pixel–pixel distance. The constitutive parameters (surface tension, noise term and lateral growth) are in the following ranges: $-0.3 \leqslant \upsilon \leqslant -0.1$, $-5.0 \leqslant \sigma \leqslant 5.0$ and $\lambda$ without restriction and the $\eta(x,t)$ is a directional Gaussian noise term. More details on the nano-KPZ sample (nKPZ) showed in Fig. 1d are given in Baroni et al. [10].

## 3. Characterization of structural complexity

At present, since spatial information is ever more accessible through high resolution digitized images, the need for robust methodologies for complex pattern characterization is obvious. Considerable attention has been drawn to spatially extended structures in real space where the characterization of pattern formation is a remarkable challenge. In this sense, many useful mathematical and statistical approaches have been proposed ([4,20,21] and references therein). Motivated by the porous silicon investigation described before, in this section, we introduce an alternative and complementary approach for characterization of connectivity and asymmetrical fluctuation along the characteristic lengths of a given disordered surface. The combination of both structural properties is proposed as an effective measurement for structural complexity. Note that a reference sample should be, from a phenomenological point of view, compatible to the samples whose structural pattern must be characterized. In principle, a phenomenological compatibility should take in consideration the scaling and universality of the dynamical processes involved. The Au-on-mica (Au-mica, for simplicity) was chosen due to its compatibility to the process involved here: stochastic surface formation on nanometric crystalline substrates.

### 3.1. The Euler characteristic

The theory of integral geometry offers a concise way of dealing with boundaries and extended connectivity in irregular structures. For a surface embedded in a volume, the Euler characteristic, $\chi$, is defined as the integral over the boundary curvature, extended along the entire boundary [4]. Thus, this measure can be interpreted also as the connectivity of a structure, being very appropriate to SFM porous silicon samples due to the presence of local walls (see Fig. 1a). While most existing measurement methodologies of $\chi$ use a generalized Boolean grain model constructed around a set of points, a complementary approach using density or amplitude random fields is also possible. In our approach, for given irregular amplitude field distributed in a 2D integral scale $L \times L$, it is taken as the excursion set of all points above a certain aspect ratio threshold, $\Gamma = r/L$, and measures the Euler characteristic as function of this threshold, being $r$ the linear local scale of a given amplitude distribution:

$$\chi(\Gamma) = \left(\frac{1}{2\pi}\right)(\Gamma - \Gamma_0)\exp\left[-\frac{1}{2}(\Gamma - \Gamma_0)^2\right], \tag{2}$$

where $\Gamma_0$ denotes the characteristic length of the correspondent binary global structure.

By determining the Euler characteristic for every disordered sample shown in Fig. 1, we can characterize the correspondent connectivity profile, as shown in Fig. 2. Here, the interesting question arises on the structural complexity of each sample. Thus it is defined that the sample GM08 is the most ordered one among all samples investigated in this paper, being the reference pattern from where a degree of relative structural complexity can be estimated. Thus, it makes sense to introduce the *relative connectivity* as being

$$\delta_M\left(\frac{\chi}{\chi^*}\right) = \frac{1}{M}\sum_{m=1}^{M}\chi_m \ln\left(\frac{\chi_m}{\chi_m^*}\right), \tag{3}$$

where $\chi^*$ is the reference *connectivity* profile (here, for the GM08 sample) and $\chi$ is the discrete *connectivity* profile to be characterized (here, samples 28 and 101 of piSi and nKPZ). Note that this measure holds for a set of $M$ connectivity values, where $m$ is the index for each value representing the connectivity for different scales of the sample. The measure given by formula (3) is based on the concept of relative entropy (or *Kullback–Leibler distance*) [22], defined here as a normalized mutual information distance. The relative connectivity for porous silicon and nKPZ samples are listed in Table 2.

### 3.2. Gradient spectra

The GPA characterizes extended patterns based on large and small amplitude fluctuations of the spatial, temporal, and spatio-temporal structures represented as a static or dynamical gradient lattice [2,3,10–18,23].

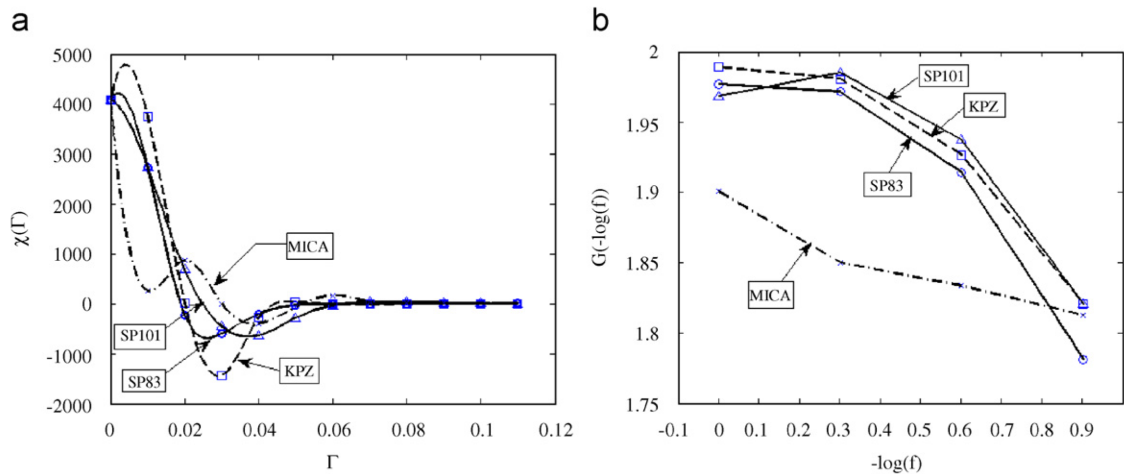


Fig. 2. (a) The Euler characteristics $\chi(\Gamma)$ and (b) the asymmetry spectra of the samples which are shown in Fig. 1. In part (a), the solid and dashed lines mark spline fittings to the data just to identify and stress the different functional behaviors for the samples.

Table 2
Relative structural complexity for SFM-PS and nKPZ surfaces

| Sample | $W$ (%) | $\delta\ (\chi/\chi^*)$ | $\delta\ (G/G^*)$ | $\rho_{SC}$ |
|---|---|---|---|---|
| SP83 | 52 | 1.978 | 0.063 | 2.041 |
| SP101 | 74 | 2.134 | 0.080 | 2.214 |
| nKPZ | 86 | 3.565 | 0.082 | 3.647 |

The local fluctuation, between each pair of amplitudes of the global pattern is characterized by its gradient vector at corresponding mesh-points in the 2D space. In this representation, the relative values between adjacent amplitudes (“local fluctuations”) are relevant, rather than the respective absolute values. Thus, according to the GPA methodology [15], the first gradient moment, $g_1$, a measurement of asymmetric fluctuation called here *asymmetry coefficient G*, is given by

$$G = \frac{|\varepsilon - f|}{f}, \quad \varepsilon > f > 0, \tag{4}$$

where $f$ is the number of asymmetric fluctuations and $\varepsilon$ is the geometric energy correlation given by the number of connections among all fluctuations. The geometric connection among the fluctuations is generated by a *Delaunay triangulation*, taking the middle points of the asymmetric vectors as vertices [11]. Due to the possible changes in the phases of each fluctuation (a vector in the gradient lattice), the parameter $\varepsilon$ is very sensitive in detecting local asymmetric fluctuations on the gradient lattice [11]. Note that in a gradient field such relative values can be characterized by each local vector norm and its orientation (phase). In this approach, each local fluctuation is represented by a vector in a 2D space. The asymmetry coefficient $G$ is intrinsically calculated on the amplitude differences (fluctuations) given by the gradient pattern of the spatial structure. As the asymmetry coefficient is very sensitive to small changes in the phase and modulus of each fluctuation vector, it can distinguish complex variability patterns even when they are very similar and consist of a low amount of vectors. Once the 2D spatial patterns can be decomposed into different frequency sub-bands, it may be interesting to characterize a gradient spectrum by calculating the asymmetry coefficient for the sub-matrices that can be obtained from such scaling decomposition.

In order to analyze the asymmetries of given spatial pattern and its correspondent sub-patterns, we consider a two-variable wavelet multi-resolution analysis (WMA) in 2D space that, without the loss of generality, can decompose a spatial pattern into different frequency bands or scaling components, so that each decomposed frame can be analyzed for its resolution scale. Here, we use the decomposition methodology introduced by

Guan et al. [20]. Each original pattern can be described by a scalar field from where 2D subspaces can be divided into LL, LH, HL and HH components (H for *high-pass* and L for *low-pass*), so that appropriate basis functions for each wavelet subspace can be constructed as the product of 1D basis functions. Thus, in our approach, an image or a pattern is a square integrable function that can be decomposed into appropriate subspace components characterized by the frequencies $f_{\max}$, $f_{\max}/2$ ($HH_3$), $f_{\max}/4$ ($HH_2$), and $f_{\max}/8$ ($HH_1$). In our notation, considering $f_{\max} = 1$, we use the reference values of 1, 0.5, 0.25 and 0.125. As we have a sub-matrix for each one of the frequencies, we can calculate the asymmetry coefficient as a function of $f$, generating the following spectra: $G$:{$G(1)$, $G(0.5)$, $G(0.25)$, $G(0.125)$}, that we call *gradient spectrum*. Thus, at this point, it may be interesting to compare the gradient spectrum of each sample shown in Fig. 1 (see Fig. 2b). Therefore, from the same considerations for connectivity, it makes sense to introduce the *relative spectral asymmetry* as

$$\delta\left(\frac{G}{G^*}\right) = \frac{1}{4}\sum_{m=1}^{4} G_m \ln\left(\frac{G_m}{G_m^*}\right), \tag{5}$$

where $G^*$ is the reference gradient spectrum (here, for the GM08 sample) and $G$ is the discrete gradient spectrum profile to be characterized (here, samples 28 and 101 of piSi and nKPZ). The *relative spectral asymmetry* for porous silicon and nKPZ samples are listed in Table 2, and for the purpose of structural complexity characterization, the measurements given by Eqs. (4) and (5) can be interpreted and tested as complementary tools. Thus, we define the *relative structural complexity*, $\rho_{SC}$, in the simplest form

$$\rho_{SC} = \delta_M\left(\frac{\chi}{\chi^*}\right) + \delta_M\left(\frac{G}{G^*}\right). \tag{6}$$

It is worth to note that this measurement is depending on the reference pattern identification, which must be defined for each application. Calculated values for this proposed measurement, taking into account Au-mica substrate sample as the reference pattern, are shown in next section.

## 4. Results and interpretation

Values of $\delta(\chi/\chi^*)$, $\delta(G/G^*)$ and $\rho_{SC}$ for samples SP83, SP101, KPZ and Au–Mica are shown in Fig. 2a and b, respectively. From these measurements it is possible to calculate the relative connectivity and relative spectral asymmetries, all relative to the simplest structure, in this context, given by the Au–Mica pattern. Table 2 presents the results of all calculations applying formulas (2)–(6) on the samples analyzed here. Note that, as Au–Mica is the reference sample, it does not appear in Table 2. As a comparison criterion, the respective roughness for each sample is shown in this table. The final result points out that, among the three samples SP83, SP101 and nKPZ, the nKPZ presents the highest *relative structural complexity*. However, it is interesting to note that this occurs due to the low connectivity of this sample when compared to the Au–Mica reference sample. In the other hand, even if the samples SP83 and SP101 if are significantly different in terms of surface porosity (differing 22% between them), their connectivity are slightly different. Taking into account the scaling asymmetry fluctuations and the relative structural complexity, one can see that the nKPZ model should be improved or be used as it is here to model PS samples more complex than that. In that sense, our results work as a validation criterion for modeling. The remarkable characterization is concerning SP83, even if it is the most asymmetric sample in the global range (see Table 1), what does not happen for the local decomposed scales. Thus, based on the relative structural complexity calculated here, the SP83 pattern has less relative asymmetric fluctuations than SP101, showing that the structural complexity concept depends on the choice of a reference pattern.

## 5. Concluding remarks

Even though the discovery of PL from porous silicon has been considered an important issue in nanoscience, there have been few investigations concentrated on structural properties of this material. In this paper, our main result shows that the structural complexity of this material cannot be interpreted only in terms

of amount of roughness and/or porosity. Moreover, the porous silicon sample that has less surface porosity (SP83) and, consequently, less structural complexity (it is more spatially organized) presents a higher PL performance comparing to the sample SP101 that presents more porosity. This result puts stress on the hypothesis that the PL phenomena can be related to the complex morphological aspects and how the reminiscent crystallites from the etching process can be distributed along the local structures (pores, valleys and walls).

Motivated by the issues mentioned above, in our approach, we have introduced two new measurements that allow us to characterize disordered patterns when it is known as a reference ordered pattern. The first measurement, based on integral geometry, search for complex local structures as irregular walls and valleys, while the second measurement, based on convex geometry, searches for asymmetric fluctuation in the characteristic scales that compose the main pattern. Even though it is possible to exist similarities and redundancies in some level, both measurements, in their relative forms, are complementary in the framework of characterizing structural complexity. In particular, in the scope of this approach, other experimental data [24–26] and also other proposed modeling of PS formation process can be analyzed (e.g., Refs. [8,27,28]). Of great interest is that the PL from PS has been associated with a variety of structural mechanisms [29–33].

Further improvement of this methodology and analysis, which could lead to more precise structural complexity characterization, might involve other reference patterns as random (Gaussian and non-Gaussian fluctuations), turbulent [34], chaotic dynamics [35,36], ballistic deposition [5], sine combination surfaces [8], among others.

## Acknowledgments

The work was financially supported by INPE-MCT and CNPq. The authors acknowledge EMBRAPA for the Au–Mica sample.

## References

[1] A.M. Albano, P.E. Rapp, N.B. Abraham, A. Passamante (Eds.), Measures of Spatio-Temporal Dynamics,, North-Holland & Elsevier, Amsterdam, 1996.
[2] R.R. Rosa, C.R. Neto, F.M. Ramos, A.S. Sharma, J.A. Valdivia, European Physical Society, EPS—Modeling Collective Phenomena in Complex Systems, vol. 22F, 1998b, pp. 304–305.
[3] R.R. Rosa, A.S. Sharma, J.A. Valdivia, H.S. Sawant, Physica A 257 (1998) 509–514.
[4] K.R. Mecke, D. Stoyan (Eds.), Lecture Notes in Physics, vol. 554, 2000, pp. 1–413.
[5] A.-L. Barabasi, H.E. Stanley, Fractal Concepts in Surface Growth, Cambridge, 1995.
[6] J. Krug, H. Spohn, Phys. Rev. Lett. 64 (1990) 2232–2235.
[7] C.-H. Lam, L.M. Sander, Phys. Rev. Lett. 69 (1992) 3338–3341.
[8] J.B. DaSilva Jr., E.A. Vasconce, B.E.C.A. dos Santos, J.A.K. Freire, V.N. Freire, G.A. Farias, E.F. da Silva Jr., Microelectron. J. 36 (2005) 1011–1015.
[9] M. Kardar, G. Parisi, Y.-C. Zhang, Phys. Rev. Lett. 56 (1986) 889–892.
[10] M.P.M.A. Baroni, R.R. Rosa, A.F. Silva, I. Pepe, L.S. Roman, F.M. Ramos, R. Ahuja, C. Persson, E. Veje, Microelectron. J. 37 (2006) 290–294.
[11] R.R. Rosa, A.S. Sharma, J.A. Valdivia, Int. J. Mod. Phys. C 10 (1999) 147–163.
[12] R.R. Rosa, J. Pontes, C.I. Christov, F.M. Ramos, C.R. Neto, D. Walgraef, Physica A 283 (2000) 156–159.
[13] F.M. Ramos, R.R. Rosa, C.R. Neto, A. Zanandrea, Physica A 283 (2000) 171–174.
[14] C.R. Neto, A. Zanandrea, F.M. Ramos, R.R. Rosa, M.J.A. Bolzan, L.D.A. Sá, Physica A 295 (2001) 215–218.
[15] R.R. Rosa, M.R. Campos, F.M. Ramos, S. Fujiwara, T. Sato, Braz. J. Phys. 33 (2003) 605–609.
[16] A. Ferreira da Silva, R.R. Rosa, L.S. Roman, E. Veje, I. Pepe, Solid State Commun. 113 (12) (2000) 703–707.
[17] A. Ferreira da Silva, R.R. Rosa, P.W.A. Machado, F.M. Ramos, C.R. Neto, L.S. Roman, E. Veje, Physica A 283 (2000) 223–227.
[18] M.P.M.A. Baroni, R.R. Rosa, L.S. Roman, A. Ferreira da Silva, 13th Brazilian Workshop on Semiconductor Physics, pp. 100–101, April 1–5, 2007, São Paulo, Brazil.
[19] T. Kobiela, Z. Kaszkur, R. Duś, Thin Solid Films 478 (1–2) (2005) 152–158.
[20] S. Guan, C.-H. Lai, G.W. Wei, Physica D 163 (2002) 49–79.
[21] Y.P. Zhao, G.C. Wang, T.M. Lu, Characterization of Amorphous and Crystalline Rough Surfaces: Principles and Applications, Academic Press, San Diego, CA, 2001.
[22] S. Kullback, R.A. Leibler, Ann. Math. Stat. 22 (1) (1951) 79–86.
[23] A.T. Assireu, R.R. Rosa, N.L. Vijaykumar, J.A. Lorenzetti, E.L. Rempel, F.M. Ramos, L.D. Abreu Sá, M.J.A. Bolzan, A. Zanandrea, Physica D 168 (1) (2002) 397–403.

[24] D. Walgraef, Spatio-Temporal Pattern Formation, Springer, Berlin, 1997.
[25] D.B. Vasconcelos, R.L. Viana, S.R. Lopes, A.M. Batista, S.E.S. de Pinto, Physica A 343 (2004) 201–218.
[26] D.C. Chang, V. Baranauskas, I. Doi, J. Porous Mater. 7 (2000) 349–352.
[27] M. Haurylau, Mater. Sci. Eng. C 15 (2001) 117–119.
[28] M. Wesolowski, Phys. Rev. B 66 (2002) 205–207.
[29] Y.H. Xie, W.L. Wilson, F.M. Ross, J.A. Mucha, E.A. Fitzgerald, J.M. Macauley, T.D. Harris, J. Appl. Phys. 71 (1992) 2403.
[30] S.M. Prokes, J. Appl. Phys. 73 (1993) 407.
[31] M. Stutzmann, M.S. Brandt, M. Rosenbauer, H.D. Fuchs, S. Finkbeiner, J. Weber, P. Deak, J. Lumin. 57 (1993) 321.
[32] A.G. Cullis, L.T. Canham, P.D. Calcott, J. Appl. Phys. 82 (1997) 909.
[33] J.L. Gole, E. Veje, R.G. Egeberg, A. Ferreira da Silva, I. Pepe, D.A. Dixon, J. Phys. Chem. B 110 (2006) 2064–2073.
[34] F.M. Ramos, R.R. Rosa, C.R. Neto, M.J.A. Bolzan, L.D.A. Sa, H.F.C. Velho, Physica A 295 (1–2) (2001) 250–253.
[35] E.L. Rempel, A.C.L. Chian, E.E.N. Macau, R.R. Rosa, Chaos 14 (3) (2004) 545–556.
[36] A.C.L. Chian, E.L. Rempel, E.E. Macau, R.R. Rosa, F. Christiansen, Phys. Rev. E 65 (3) (2002) 035203.